Title: Modeling clinical responses to targeted therapies by patient-derived organoids of advanced lung adenocarcinoma

Seok-Young Kim[1], Sang-Min Kim[2], Sumin Lim[3], Ji Yeon Lee[3], Su-Jin Choi[1], San-Duk Yang[1], Mi Ran Yun[1], Chang Gon Kim[1], Seo Rin Gu[3], Chaewon Park[1], A-Young Park[1], Sun Min Lim[1], Seong Gu Heo[1], HyunKi Kim[2], Byoung Chul Cho[4]

SY KIM and SM KIM equally contributed as co-first authors.
BC Cho, Hk Kim, SG Heo equally contributed as co-corresponding authors.

Author affiliation

[1]Yonsei Cancer Center, Division of Medical Oncology, Department of Internal Medicine, Yonsei University College of Medicine, Seoul, Korea; [2]Department of Pathology, Yonsei University College of Medicine, Seoul; [3]Interpark Bio Convergence Corp., Seoul, Korea; [4]Yonsei Cancer Center, Division of Medical Oncology, Yonsei University College of Medicine, Seoul, Korea.

Correspondence

Byoung Chul Cho, MD, PhD, Yonsei Cancer Center, Division of Medical Oncology, Yonsei University College of Medicine, 50 Yonsei-Ro, Seodaemun-Gu, Seoul, Korea (e-mail: CBC1971@yuhs.ac); Hyunki Kim, MD, PhD, Department of pathology, Yonsei University College of Medicine, 50 Yonsei-Ro, Seodaemun-Gu, Seoul, Korea (e-mail: KIMHYUNKI@yuhs.ac); or Seong Gu Heo, MS, Yonsei Cancer Center, Division of Medical Oncology, Department of Internal Medicine, Yonsei University College of Medicine, 50 Yonsei-Ro, Seodaemun-Gu, Seoul, Korea (e-mail: LUKEHUR1@yuhs.ac).

Running title: Clinical relevance of lung cancer patient-derived organoids

Keywords: Advanced lung adenocarcinoma, patient-derived organoids, precision medicine, driver oncogene

Conflict of Interest statement

Dr. Cho is the founder of DAAN Biotherapeutics, a board of director at Gencurix Inc., Interpark Bio Convergence Corp., a consultant for Novartis, AstraZeneca, Boehringer-Ingelheim, Roche, BMS, Ono, Yuhan, Pfizer, Eli Lilly, Janssen, Takeda, MSD, Janssen, Medpacto, Blueprint medicines, and a scientific advisory board at KANAPH Therapeutic Inc., Brigebio therapeutics, Cyrus therapeutics, and Guardant Health. Dr. Cho receives research funding from Novartis, Bayer, AstraZeneca, MOGAM Institute, Dong-A ST, Champions Oncology, Janssen, Yuhan, Ono, Dizal Pharma, MSD, Abbvie, Medpacto, GIInnovation, Eli Lilly, Blueprint medicines, Interpark Bio Convergence Corp., and royalty from Champions Oncology. Dr. Cho owns stocks of TheraCanVac Inc., Gencurix Inc., Bridgebio therapeutics, KANAPH Therapeutic Inc., Cyrus therapeutics, and Interpark Bio Convergence Corp. The authors have no additional financial interests.

Translational relevance

We demonstrated that *in vitro* drug responses in patient-derived organoids (PDOs) are correlated to clinical responses to targeted therapies in individual patients with advanced lung adenocarcinoma and PDOs can be used to identify effective anti-cancer therapies for novel molecular targets. PDOs recapitulated progression-free survival and objective responses of NSCLC patients receiving clinically approved targeted agents. PDOs also predicted activity of therapeutic strategies under clinical investigation. YUO-071 harboring an *EGFR* exon 19 deletion and a *BRAF* G464A mutation and the matching patient responded to dabrafenib/trametinib combination therapy. YUO-004 and YUO-050 harboring an *EGFR* L747P mutation was sensitive to afatinib, consistent with the response in the matching patient of YUO-050. Furthermore, we utilized organoids to demonstrate preclinical efficacy of poziotinib against *ERBB2* exon 20 insertions and pralsetinib against *RET*-fusions. Our findings suggest utility of PDOs in clinical decision making and development of therapeutic strategies.

Abstract

Purpose: Patient-derived organoids (PDOs) of lung cancer has been recently introduced, reflecting the genomic landscape of lung cancer. However, clinical relevance of advanced lung adenocarcinoma organoids remains unknown. Here, we examined the ability of PDOs to predict clinical responses to targeted therapies in individual patients and to identify effective anti-cancer therapies for novel molecular targets.

Experimental design: Eighty-four organoids were established from patients with advanced lung adenocarcinoma. FFPE tumor specimens from corresponding patients were analyzed by whole-exome sequencing (n = 12). Organoids were analyzed by whole-exome sequencing (n = 61) and RNA-sequencing (n = 55). Responses to mono- or combination targeted therapies were examined in organoids and organoid-derived xenografts.

Results: PDOs largely retained somatic alterations including driver mutations of matching patient tumors. PDOs were able to recapitulate progression-free survival and objective responses of NSCLC patients receiving clinically approved tyrosine kinase inhibitors. PDOs recapitulated activity of therapeutic strategies under clinical investigation. YUO-071 harboring an *EGFR* exon 19 deletion and a *BRAF* G464A mutation and the matching patient responded to dabrafenib/trametinib combination therapy. YUO-004 and YUO-050 harboring an *EGFR* L747P mutation was sensitive to afatinib, consistent with the response in the matching patient of YUO-050. Furthermore, we utilized organoids to identify effective therapies for novel molecular targets. We demonstrated efficacy of poziotinib against *ERBB2* exon 20 insertions and pralsetinib against *RET*-fusions.

Conclusions: We demonstrated translational relevance of PDOs in advanced lung adenocarcinoma. PDOs are an important diagnostic tool which can assist clinical decision making and accelerate development of therapeutic strategies.

Introduction

Non-small cell lung cancer (NSCLC) is a leading cause of cancer-related mortality worldwide. Over the last decade, precision medicine tailored to an individual patient has greatly improved survival and disease control in patients with advanced NSCLC. Implementation of precision medicine requires identification of actionable molecular targets and treatment with therapies targeting the specific genetic aberrations (1). The molecular profiling-based drug selection has several limitations. Only a portion of NSCLC benefits from targeted therapies; molecular subsets including *EGFR* activating mutations and T790M mutation, *BRAF* V600E mutation, *MET* exon 14 skipping mutations, *ALK*, *ROS1*, *RET,* and *NTRK1/2/3* fusions (2). Additionally, responses to targeted therapies are heterogeneous in patients harboring the identical driver mutation (3-5). Rarer molecular subtypes among the driver oncogenes display diverse clinical and biological characteristics, further complicating the clinical decision making for patients with advanced NSCLC (6-9).

Recent studies have focused on patient-derived organoids (PDOs) as preclinical models to investigate tumor biology. PDOs are tissue specific stem cells derived from various adult human organs and cancers. The organoids have been cultured in three-dimensional (3D) conditions utilizing extracellular matrix components (10). Although 2D conventional cell lines have been widely used in cancer research, they may not represent complex biological characteristics of patient tumors. Furthermore, establishment and utilization of 2D patient-derived cells which represents their parental tumors has been hampered by a low success rate for model establishment (11). Additionally, classical *in vivo* models are time consuming, labor-intensive and limiting the high-throughput studies (12). Notably, PDOs have short established time and retain biological features of the patient tumors, presenting unique value for precision medicine.

Previous studies on NSCLC PDOs have utilized primary patient tumors and patient-derived xenografts of early-stage NSCLC including lung squamous cell carcinoma, lung adenocarcinoma, and large cell carcinoma (13-16). In this study, we establish PDOs using malignant effusions and metastatic surgical specimens of advanced lung adenocarcinoma and demonstrate that PDOs are a clinically-relevant platform which can be used for patient-specific drug testing and proof of concept preclinical studies.

Materials and methods

Patient consent and samples

This study was approved by Yonsei University Hospital Institutional Review Board (Seoul, Korea) (IRB no.: 4-2016-0788) and conducted in accordance with the Declaration of Helsinki. All patients provided written informed consent. Pleural effusion and surgically resected metastatic tumors were collected from patients with advanced lung adenocarcinoma at Yonsei Cancer Center. Fluorescence in situ hybridization (FISH), direct sequencing, TruSight Oncology 500 (Illumina, CA, USA), or TruSight Tumor 170 (Illumina) was performed for molecular profiling of NSCLC at initial diagnosis or at recurrence. Cell-free DNA (cfDNA) of matching patient for YUO-071 (Guardant Health, CA, USA) was analyzed using Guardant360® assay.

Processing of malignant effusions

In order to standardize the experimental protocol, only 200 mL of malignant effusion was used to collect tumor cells. Red blood cells in the cell pellet were removed by hypotonic lysis in sterile MilliQ H2O (Merk Millipore, MA, USA) followed by adding Advanced DMEM/F12 medium (Gibco, MA, USA), being strained over a 100 µm filter with retained debris, and centrifuged at 500 g for 5 min.

Surgical tumor tissue processing

Tumor tissue washed three times with advanced DMEM/F12 supplemented with antibiotics (Invivogen, CA, USA) and chopped with sterile blades. Tumor pieces were dissociated in 2 mg/mL collagenase (Sigma-Aldrich, MO, USA) on shaker at 37°C for 1-2h. After incubation, the suspensions were added with advanced DMEM/F12 medium, passed through 100 µm cell strainers, and centrifuged at 500 g for 5 min.

Establishment of organoids

Organoids were established as previously described (15). In brief, cells were counted under a microscope and centrifuged at 500 g for 5 min. Then, cells were resuspended in ice-cold 500 µL Matrigel (Corning, NY, USA) and 20 µL drops of Matrigel cell suspension were seeded on pre-warmed 48-well culture plates (Corning) at a density of ~2 X 10^3 cells per 20 µL Matrigel/well. The Matrigel was solidified for 15 min at 37°C and overlaid with 250 µL airway organoid medium (AO) (AdDF+++, 20% conditioned R-spondin1 medium supplemented with B27 (Invitrogen, CA, USA), 1.25 mM N-Acetylcystein (Sigma-Aldrich), 5

mM nicotinamide (Sigma), 25 ng/ml human fibroblast growth factor 7 (Peprotech, NJ, USA), 100 ng/mL human noggin (Peprotech), 100 ng/mL human fibroblast growth factor10 (Peprotech), 500 nM A83-01 (Tocris, Bristol, UK), 500 nM SB202190 (Sigma)). AdDF+++ medium is Advanced DMEF/F12 medium (Invitrogen) supplemented with 10 nM HEPES (Invitrogen), 1X GlutaMax (Invitrogen), and 1X Antibiotic-Antimycotic (Invitrogen). 10 µM Y-27632 (Enzo Life Science, NY, USA) was added for the first 2 days. Cultures were kept at 37°C, 5% CO2 in a humidified incubator. Medium was replenished every 2-3 days.

Histology and immunohistochemistry

Organoids and their parental tumors were fixed in 4% paraformaldehyde for 24h at 4°C, washed with phosphate-buffered saline (PBS) and then transferred to 70% ethanol, processed for paraffin embedding, sectioning, deparaffinization, dehydration, and hematoxylin-eosin staining. Immunohistochemistry was performed using the antibody against thyroid transcription factor 1 (TTF-1, Clone EP1584Y, Abcam, Cambridge, UK), Calretinin (Clone DAK-Calret-1, Agilent Technologies, CA, USA), and p53 (Leica Biosystems, Wetzlar Germany). Organoid imaging was performed on OLYMPUS BX51 microscope (Olympus, Tokyo, Japan) using a 20× magnification. Images were processed using Olympus cellSens software and Photoshop CS4 (8 bit).

Next-generation sequencing

RNA was isolated from organoids using TRIzol (Invitrogen) following the manufacturer's instructions. RNA libraries were generated from 55 patient-derived organoids using TruSeq Stranded mRNA Sample Prep Kit (Illumina, CA, USA). The libraries were subjected to paired-end sequencing with a 150 bp read length using NovaSeq 6000 (Illumina). Quality scores for over 75% of raw reads were >Q30. We used Arriba (https://github.com/suhrig/arriba/), which is based on the STAR aligner, to detect fusion genes in organoids. A minimum coverage fraction of Arriba is 0.15, ignoring the fusion events that are not fully expressed. GENCODE19, hs37d5, blacklist_hg19_hs37d5_GRCh37 assembly and annotation files were used. The circos plots from RNA-seq data of fusion transcript candidates with highest coverage was drawn.

Genomic DNA (gDNA) was isolated from organoids, matching normal blood samples and formalin-fixed paraffin-embedded (FFPE) tumor specimens using the DNeasy Blood & Tissue kits (Qiagen, Venlo, Netherlands). Concentration and purity of gDNA were assessed by agarose gel electrophoresis and PicoGreen® dsDNA assay (Invitrogen). Exome libraries were generated from 61 patient-derived organoids and 58 matching normal blood samples using SureSelect v6 kit (Agilent Technologies, CA, USA) and sequenced on NovaSeq

(Illumina). Sequencing reads were mapped to the human chromosome (hg19) using the Burrows-Wheeler alignment tool (17, 18). Somatic mutations in each tumor specimen or organoid were detected using MuTect2 and annotated with Oncotator (19). High quality somatic mutations were acquired by i) filtering out germline mutations with allele frequencies > 0.01 in the Exome Aggregation Consortium (ExAC) database, ii) filtering out somatic mutations with allele frequencies < 0.01, and iii) including mutations in the cosmic database. Copy number variations were detected using CNVkit (20).

Clinically-relevant somatic alterations were selected based on the TARGET database (21). 'Actionable targets' and 'Clinically-relevant driver genes' were selected based on the NCCN guideline (version 8. 2020) and the lung adenocarcinoma TCGA database (2). Specifically, 'Actionable targets' were defined as driver oncogenes in lung adenocarcinoma which clinically respond to FDA-approved targeted agents, including *EGFR* L858R mutation, exon 19 deletions, T790M mutation, G719X mutation, S768I mutation, L861Q mutation, *ROS1* fusions, *RET* fusions, and *BRAF* V600E mutation. We were not able to detect *ALK*- and *NTRK* fusions in our organoid library. 'Clinically relevant driver genes' were defined as driver oncogenes in lung adenocarcinoma that are under clinical investigation for druggability, including *MET* amplification, *ERBB2* amplification, mutations in kinase domains of *ERBB2* (exon 19-21), *KRAS* (exon 2-3), *BRAF* (exon 11-18), and *EGFR* (exon 18-21) other than the aforementioned *EGFR* and *BRAF* actionable targets.

The NGS data are available at the Sequence Read Archive (accession number: PRJNA725056).

Cell viability assay

Organoids were cultured in AO medium for 5-10 days after organoids were dissociated into single cells using TrypLE (Thermo Fisher, MA, USA). 1 mg/mL dispase solution was added to plates and incubated at 37°C for 10 min before cell suspension was pipetted with a 1 mL tip few times, washed twice with cold PBS, and centrifuged at 1300 rpm for 3 min. Organoid pellets were resuspended in AdDF+++ medium containing 5% Matrigel, seeded on 96-well ultra-low attachment plates (Corning, NY, USA) (2500 organoids/well), and treated with drugs after 1h (22). At indicated time points, CellTiterGlo 3D (Promega, WI, USA) was used to measure luminescence according to the manufacturer's protocol.

For 2D cultures, cells were seeded on 96-well plates in AdDF+++ medium (5000 cells/well) (7). After overnight incubation, AdDF+++ medium containing drugs were added to the wells. After 3 days, CellTiterGlo 3D was used to measure luminescence according to the manufacturer's protocol.

IC_{50} values were calculated from 3 biological replicates (3 technical replicates per biological replicate) using GraphPad Prism version 7. *In vitro* response to a targeted therapy was defined as sensitive (IC_{50} value < 100 nmol/L) or resistant (IC_{50} value > 100 nmol/L) (7).

Measuring change of cell viability after drug exposure

A protocol for drug exposure was based on Sharma et al. (23). Briefly, organoids were suspended in Matrigel and seeded on 48-well plates (~250 organoids/well, 3 wells per biological replicate). Organoids were replenished with fresh AdDF+++ medium containing a drug at the indicated concentration every 3 days up to 15 days. At indicated time points, medium was decanted and 200 µL CellTiterGlo 3D was added to each well. After 30 min incubation at room temperature, 100 µL used to measure luminescence. Relative cell viability was calculated as follows: (Luminescence at the indicated time point)/(Luminescence at day 0). Percentage change of cell viability was calculated as follows: [(Luminescence at the indicated time point) - (Luminescence at day 0)]/(Luminescence at day 0)*100.

Direct sequencing

Direct sequencing of *EGFR* exon 18, 19, 20, 21 was performed as previously described (7).

Model switching between 3D cultures and 2D cultures

To generate 2D cultures from 3D organoids, which we termed 2D PDO, approximately 1 X 10^6 organoid fragments were suspended in AO medium and seeded on a 100Φ collagen-coated plate. Successful 2D PDO was defined as a culture that could be passaged in monolayer condition for 1 month. An additional attempt was made for each 3D PDO that failed to generate 2D cultures. Cells were replenished with fresh AO medium twice a week. To minimize clonal selection in 2D cultures, 2D PDOs generated within 1 month were used for cell viability assays and immunoblot analysis. To generate 3D cultures from 2D PDOs, which we termed 2D-3D PDO, 2D cells were dissociated, resuspended in Matrigel, seeded at 1 X 10^5 cells per well in 24-well plates, and cultured in a similar manner to 3D PDOs.

Immunoblots

Organoids were suspended in Matrigel, plated in 24-well plates, and overlaid with AdDF+++ medium. After overnight incubation, medium was replaced with AdDF+++ medium containing a drug and incubated for the indicated times. Organoids were harvested using Cell Recovery Solution (Corning) and washed 3 times with ice-cold PBS according to the manufacturer's instructions. pEGFR (#2234), EGFR (#2232), pAKT (#4060), AKT (#4691),

pERK (#4370), ERK (#4696), pMEK1/2 (#9154), MEK1/2 (#4694), pS6 (#4858), S6 (#2217), pERBB2 (#2243), ERBB2 (#2165), Src (#2108), pSTAT3 (#9145), STAT3 (#9139), pRET (#3221), RET (#3223), pShc (#2434), Shc (#2432), and secondary antibodies (#7074 and #7076) were purchased from Cell Signaling Technology (MA, USA). pSrc (MAB2685) was purchased from R&D systems and Actin (MAB1501R) was from Merck Millipore.

Immunofluorescence

Cell strainers were used to obtain organoids with a size ranging from 20 μm to 70 μm. Organoids were suspended in Matrigel and plated on glass-bottom 24-well plates and overlaid with AdDF+++ medium containing dimethyl sulfoxide (DMSO) or 100 nmol/L trametinib plus 100 nmol/L dabrafenib. After 5 days, organoids were stained with Ki-67 (Cell Signaling Technology, #9449), Cleaved caspase 3 (Cell Signaling Technology, #9661), and Hoechst 33258 (Invitrogen). Organoids were imaged on a Leica TCS SP8 confocal microscope (25× objective). Secondary antibodies (711-296-152 and 715-096-151) were purchased from Jackson ImmunoResearch (PA, USA).

Xenograft

Animal experiments were performed in accordance with the guidelines of Institutional Animal Care and Use Committee (IACUC) and Animal Research Committee at Yonsei University College of Medicine. To generate PDO-derived xenografts, organoids were harvested from 12 wells of 24-well plates, mechanically dissociated, resuspended in 100 μL Matrigel, and subcutaneously injected into 6-week-old female BALB/c nude mice purchased from Saeronbio (Uiwang, Korea) (14). Our preliminary success rates for generating xenografts from different PDO models were 62.5% (5/8) using nude mice and 91.7% (11/12) using NOG immunodeficient mice. Tumor-bearing mice (n = 6, randomly allocated to each group) were treated once daily with vehicle, gefitinib (25 mg/kg), afatinib (25 mg/kg), or osimertinib (25 mg/kg). Tumor samples were collected 2 hours after 30 days of treatment and subjected to immunoblot analysis. Percentage change in tumor volume was calculated as follows: $(V_t - V_0)/V_0*100$. V_t is the tumor volume of mouse treated with a drug for time t and V_0 is the tumor volume of mouse at the beginning of the study. Tumor growth inhibition (TGI) was calculated as follows: $[1 – (TV_t - TV_0)/(CV_t - CV_0)]*100$. T*V* is the tumor volume of mouse treated with a drug and C*V* is the tumor volume of mouse treated with vehicle (24).

Drugs

Drugs were purchased from SelleckChem (Texas, USA). Most drugs were dissolved in DMSO while cetuximab was dissolved in phosphate buffered saline for *in vitro* cell viability assays.

Statistical analysis

Data are presented as the mean ± SEM unless indicated otherwise. Data were analyzed using the student-*t* test, the Mann-Whitney U test, or one-way ANOVA followed by the Dunnett test.

Results

Establishment and genomic characterization of PDOs from advanced lung adenocarcinoma

From June 2018 to March 2020, we established 83 tumor organoids (77 from malignant effusions, 3 from brain metastasis, 1 from bone metastasis, and 2 from lung primary tumor) at a success rate of 83.0% (83/100) and 1 normal-like organoid from patients with NSCLC. The organoids could be maintained for 2-3 months without changes in morphology (Figure 1A and Supplementary Figure 1). Seventeen samples failed in expansion due to lack of tumor cells in effusions, fungi contaminations, and excessive immune cells.

To determine genomic landscape, whole exome sequencing (WES) and RNA-sequencing were performed on organoids with robust cell growth (n = 61 and 55, respectively) (Figure 1B). Clinical annotations of these organoids are summarized in Supplementary Table 1. Of 60 tumor organoids, 54 harbored lung cancer driver oncogenes including *EGFR* mutations (n = 34), *MET* amplification (n = 10), *ERBB2* mutations/amplification (n = 8), and *KRAS* mutations (n = 6) (22). *EGFR* and *MET* amplification co-occurred with EGFR mutations and were enriched in TKI-resistant models compared with TKI-naïve models. WES also revealed *FGFR1* amplification and *PIK3CA* mutations, known mechanisms of TKI resistance, as well as potential candidates including *MYC* and *MCL-1* amplification (21, 25). YUO-053, a normal-like organoid, did not harbor *bona fide* tumorigenic mutations.

We examined the ability of PDOs to recapitulate genetic alterations of corresponding tumors. Of 41 cases where genetic tests were performed, driver mutation status of organoids (38/41; 92.7%) was largely concordant to that of corresponding tumors detected by routine testing (n = 35) and/or targeted next-generation sequencing (NGS) (n = 9). In 2 out 3 discordant cases, organoids (YUO-048 and YUO-055) harbored additional driver mutations (HER2 exon 20 insertion and ROS1 fusion, respectively) that were not detected in matching patient tumors, possibly due to cross-cell contamination. Notably, YUO-004 harbored an *EGFR* L747P mutation, suggesting the matching patient had been misdiagnosed with EGFR exon 19 deletion due to the limitation of PCR genetic tests (26). YUO-020, YUO-041, and YUO-077 retained *ROS1*- or *RET*-fusion genes detected at the initial diagnosis (Supplementary Table 1 and Supplementary Figure 2A). Additionally, we performed WES on 12 archival FFPE tumor specimens and compared with matching PDOs (Supplementary Figure 2B and C). Somatic alterations found in the archival materials were largely preserved in PDOs (Supplementary Figure 2B and C). Despite the similarity, some (3/11; 27.3%) tumors contained low number of single nucleotide variants (SNV), insertion/deletion (Indel),

and obscure copy number variations (Supplementary Figure 2C and D). In 2 archival samples, *EGFR* driver mutations were missed possibly due to low tumor contents, although they were detected by routine testing and organoids (YUO-006 and YUO-016) (Supplementary Figure 2D and E). These results show that PDOs faithfully reflect genetic characteristics of advanced lung adenocarcinoma.

Predictive values of advanced lung adenocarcinoma PDOs

Patients with NSCLC harboring an actionable mutation generally progress to a TKI within 9 to 10 months (3, 4, 27). We tested if PDOs can recapitulate clinical outcomes in patients receiving clinically approved TKIs. First, we compared *in vitro* responses (IC_{50}) to TKI monotherapy with a progression-free survival (PFS) in patients with *EGFR*-mutant- (n = 8) or *ROS1*-positive NSCLC (n = 1), where follow-up was available (Figure 2A, Supplementary Figure 3, and Supplementary Table 2) (28). Five patients achieved a PFS of > 9 months and 4 out of 5 matching PDOs were sensitive to the TKI (IC_{50} < 100 nmol/L). Three patients had a PFS of < 9 months and 2 out of 3 matching PDOs were resistant to the TKI (IC_{50} > 100 nmol/L). One patient (YUO-067) was still on osimertinib at the data cutoff. Overall, PDOs were able to predict PFS at an accuracy of 75.0% (Figure 2B and Supplementary Table 2).

Next, we assessed the ability of PDOs to reflect response evaluation criteria in solid tumors (RECIST), an important indicator of tumor burden change and drug efficacy in the clinic (29). We exposed each organoid to a single dose of the relevant drug for 3 days and measured changes in cell proliferation (Figure 2C). Interestingly, regression of cell growth was observed in most organoids (5/6; 83.3%) established from patients who achieved a partial response, with the exception of YUO-007 that was established from a patient with a short PFS of 4.8 months on ceritinib. On the other hand, cell growth was observed in most organoids (2/3; 66.0%) established from patients who achieved stable disease. We noted that *in vitro* drug responses in YUO-030 were not correlated to both PFS and RECIST of the matching patient (Supplementary Table 2). The median change of cell viability was distinguishable between the 2 groups (-23.3% vs 16.8%). Together, these data demonstrate that *in vitro* drug responses in PDOs are correlated to clinical outcomes in patients with oncogene-driven NSCLC treated with systemic therapy.

Comparison of clinical relevance in 3D and 2D culture conditions

2D cultures have been widely used for translational research (7, 11). To directly compare clinical relevance of 2D cultures and organoids, we attempted to generate 2D cultures from 9 PDOs with known clinical responses to TKIs (2D PDO, designated with a '2D' prefix to the model identifier) (Figure 3A). We established 2D PDOs with a success rate of 55.5% and

assessed IC_{50} values of the relevant drugs in these models (Supplementary Figure 4A). Intriguingly, some 2D PDOs (2/5: 40.0%) exhibited differential TKI sensitivity to their 3D counterparts, of which 1 (1/2: 50.0%) failed to capture the clinical response (Figure 3B and Supplementary Table 2). We examined whether selection of a driver mutation in the 2D culture influenced TKI sensitivity. Sanger sequencing analysis revealed that 2D YUO-004 retained the driver mutation at a similar mutation allele frequency (Figure 3C). To confirm that culture condition is the determinant of drug sensitivity in YUO-004, we switched the 2D cultures into 3D cultures (2D-3D PDO, designated with a '2D-3D' prefix to the model identifier) (Figure 3D) (30). 2D-3D YUO-004 displayed increased IC_{50} value of gefitinib, recapitulating the clinical response. Conversely, YUO-050 maintained an *EGFR* L747P mutation in 2D culture condition and was resistant to gefitinib across different culture conditions (Figure 3C and E). Additionally, 3D and 2D cultures of YUO-050 and YUO-004 were sensitive to afatinib, although the IC_{50} value of afatinib in 2D culture was slightly increased (YUO-050) or decreased (YUO-004) compared with the corresponding 3D culture (Supplementary Figure 4B).

Culture condition modulates expression or activation of HER family kinases and impacts drug sensitivity in cancer cell lines driven by EGFR or ERBB2 (31, 32). Therefore, we examined whether HER family signaling components are associated with culture conditions in YUO-004. Compared with 3D cultures, EGFR and ERBB2 phosphorylation was decreased in 2D YUO-004 and the opposite pattern was observed for YUO-050 (Figure 3F). Surprisingly, Src and STAT3 phosphorylation was significantly decreased in 2D YUO-004 compared with the 3D counterpart, whereas the difference was negligible between 2D and 3D culture of YUO-050 (Figure 3G). Src cross-activates with EGFR and combined EGFR and Src inhibition has synergistic anti-cancer effects on EGFR-dependent cancers (33, 34).Thus, we examined the effect of Src activation in YUO-004. Although dasatinib, a highly selective Src inhibitor, had no effects on YUO-050, treatment of dasatinib sensitized YUO-004 to gefitinib (Figure 3H and I) (35). Similar results were observed for 2D-3D YUO-004 which regained high phosphorylation levels of Src and STAT3 (Supplementary Figure 4C and D). These data illustrate that YUO-004 requires 3D culture-dependent Src activation to predict the clinical response.

Predictive values of PDOs in diverse clinical settings

Next, we tested the ability of organoids to predict activity of novel therapeutic strategies that are under clinical investigation. Patients with *EGFR*-mutant NSCLC progressing to osimertinib acquire heterogeneous mechanisms of resistance including a *BRAF* V600E mutation (25). Effective treatments for NSCLC harboring both *EGFR* mutation and *BRAF*

mutation remain to be elucidated. In our study, a patient with NSCLC harboring an *EGFR* exon 19 deletion and T790M mutation progressed to osimertinib (Supplementary Table 1). To select subsequent treatments, targeted NGS analysis was performed on tissue and liquid biopsies and identified *BRAF* G464A, *BRAF* V600E, and *EGFR* C797S mutations as potential druggable targets (Figure 4A). Based on these results, the patient was initiated on dabrafenib/trametinib combination therapy, an approved treatment for *BRAF* V600E-mutant NSCLC (5). Compared with a computed tomography (CT) scan prior to the combination therapy, a follow-up CT scan obtained after 1 week of the treatment demonstrated marked reduction in tumor size (Figure 4B). Unfortunately, the patient suddenly expired because of a cerebrovascular accident unrelated to disease progression after 2.5 weeks on the treatment. Simultaneously, we performed WES and cell viability assays on YUO-071 generated from malignant effusion resistant to osimertinib. YUO-071 retained the *EGFR* activating mutation and *BRAF* G464A mutation similar to the tissue NGS findings (Figure 4A). Interestingly, YUO-071 responded to trametinib with or without dabrafenib but was resistant to osimertinib, cetuximab, brigatinib and cetuximab/brigatinib combination which had demonstrated preclinical efficacy against *EGFR* exon 19 deletion/T790M/C797S mutations (Figure 4C) (36). Long-term exposure to trametinib plus dabrafenib achieved 74% organoid growth inhibition, whereas osimertinib, cetuximab, brigatinib, and cetuximab plus brigatinib resulted in organoid growth (Figure 4D). Additionally, the trametinib/dabrafenib combination drastically decreased Ki-67 and increased cleaved caspase 3 (Figure 4E and F). Considering the presence of multiple BRAF clones in the patient tumors, however, it remains to be determined which BRAF mutation (V600E and/or G464A) is responding to the combination therapy in this patient (Figure 4A). Together, these findings demonstrate that PDOs capture the clinical response to the dabrafenib/trametinib combination therapy in a patient with NSCLC harboring *EGFR* plus *BRAF* mutations.

EGFR activating mutations respond to 1st generation EGFR-TKIs, while rare *EGFR* mutations exhibit differential sensitivity to the therapies (4, 6, 7). Clinical and preclinical data regarding an *EGFR* L747P mutation are sparse (37). To identify effective therapies against the *EGFR* L747P mutation, we screened clinically available EGFR-TKIs in YUO-004 and YUO-050 established from *EGFR* L747P-mutant NSCLCs resistant to gefitinib (Supplementary Table 1 and 2). YUO-004 and YUO-050 were sensitive to 2nd generation EGFR-TKIs (dacomitinib and afatinib) but resistant to 1st (gefitinib and erlotinib) and 3rd generation EGFR-TKIs (osimertinib and lazertinib) (Figure 5A). Compared with gefitinib and osimertinib, afatinib potently inhibited EGFR downstream signaling components (Figure 5B). Afatinib induced modest growth delay with 51.8% tumor growth inhibition (TGI) in YUO-004 xenografts accompanied by marked inhibition of EGFR phosphorylation, whereas gefitinib

and osimertinib had no anti-cancer effects (TGI = 20.6% and 27.4%, respectively) (Figure 5C and D). Corroborating these findings, the matching patient for YUO-050 responded to afatinib and achieved PFS of 9.5 months (Supplementary Table 2). Together, these results demonstrate that afatinib is more potent than 1st and 3rd gen. EGFR-TKIs against the *EGFR* L747P mutation.

PDOs can identify effective anti-cancer therapies for novel molecular targets

ERBB2 mutations and *RET* fusions are emerging targets for targeted therapies, which are found in approximately 2% of patients with NSCLC (1). We utilized organoids to investigate effective targeted therapies for *ERBB2*-mutant and *RET*-rearranged NSCLC. Poziotinib, an experimental drug for treatment of *ERBB2*-mutant NSCLC, was the most potent TKI against *ERBB2* G778_779insCPG and A775_G779insYVMA insertions (Figure 6A) (38). Compared with other ERBB2 inhibitors, poziotinib more potently suppressed ERBB2-ERK-AKT signaling pathway (Figure 6B). Cells expressing wild-type target proteins can be used to determine selectivity of a targeted therapy for mutant target proteins (14, 38). Using the normal-like organoid (YUO-053) which is devoid of tumorigenic mutations (Figure 1B), we found that poziotinib had a trend to more mutant-selective than other drugs (Figure 6C and D). Additionally, pralsetinib, a highly potent inhibitor for *RET*-mutant and -rearranged tumors, was more effective than vandetanib, lenvatinib, and cabozantinib against *CCDC6-RET* fusion and *KIF5B-RET* fusion in cell viability assays and immunoblot analysis (Figure 6E and F) (39). Pralsetinib was more mutant-selective than other RET targeted therapies (Figure 6G and H). These findings underline preclinical efficacy of poziotinib and pralsetinib against NSCLCs harboring *ERBB2* exon 20 insertions and *RET* fusions, respectively.

Discussion

Tumor organoids reflect genetic alterations of tumors they were derived from and can be used to investigate drug-gene interactions (14-16, 28, 40). Importantly, PDOs of colorectal cancer, head and neck cancer, gastrointestinal cancer, and rectal cancer have been shown to predict clinical responses to not only chemoradiotherapies but also targeted therapies, bringing new insight into clinical utility of organoids (28, 29, 40, 41). Compared with previous studies on lung cancer PDOs (14-16), we correlated *in vitro* drug responses in PDOs to clinical responses in matching patients and assessed preclinical efficacy of targeted therapies under clinical development, demonstrating clinical relevance of NSCLC PDOs.

It is generally perceived that 3D cultures better reflect *in vivo* physiology than 2D cultures. In the context of *EGFR*- or *ERBB2*-driven cancer, previous studies used conventional cell lines to investigate physiological differences between 2D and 3D cultures (31, 32). For

example, Breslin et al. showed that 3D cultures of ERBB2-overexpressing cancer cells, when compared with their 2D counterparts, display increased expression and activation of HER family kinases and resistance to HER targeted drugs (31). However, *in vivo* or clinical relevance of these observations were not demonstrated. In our study, we compared predictive values between 2D and 3D cultures of clinically annotated patient-derived models and showed potential advantages of 3D organoids in translational research. Particularly, we show that 3D organoids may capture unique information such as Src activation which is not represented by neither genetic tests nor 2D cultures. We noted that some 3D PDOs (4/9: 44.4%) cannot be cultured in the monolayer condition, indicating some NSCLC may grow only as suspension cells or require extracellular matrix for optimal growth (42, 43).

In this study, we utilized organoids to assess clinical activity of novel therapeutic strategies. We demonstrate that dabrafenib/trametinib combination therapy elicits *in vitro* and clinical responses in a NSCLC harboring an *EGFR* exon 19 deletion and a *BRAF* G464A mutation. Accordingly, Ho et al. have shown that a cancer cell line harboring both *EGFR* activating mutation and *BRAF* V600E mutation is dependent on BRAF-MEK pathway and responds to a BRAF inhibitor monotherapy (44). *BRAF* G464A mutation belongs to a non-V600E *BRAF* mutation which may exhibit different clinical and molecular characteristics to the *BRAF* V600E mutation (8, 9). Our findings are in keeping with several preclinical studies and case reports which have demonstrated efficacy of trametinib with or without dabrafenib against non-V600E *BRAF* mutation (7, 9, 45). Moreover, we report preclinical and clinical efficacy of afatinib against the rare *EGFR* L747P mutation (37). Our findings and few case reports suggest that the *EGFR* L747P mutation is resistant to gefitinib and osimertinib but respond to afatinib (37, 46). These results demonstrate that organoids in addition to the molecular profiling can be a powerful diagnostic tool for precision medicine in diverse clinical settings.

Finally, we identify poziotinib as the most potent agent, among ERBB2 targeted therapies tested, against *ERBB2* exon 20 insertions that are currently without approved inhibitors. Poziotinib has demonstrated better preclinical and clinical efficacy than erlotinib, lapatinib, neratinib, and afatinib against the *ERBB2* exon 20 insertions (38, 47, 48). Additionally, we show that pralsetinib is more effective than multi kinase inhibitors vandetanib, cabozantinib, and lenvatinib. The multi kinase inhibitors had limited clinical efficacy in *RET*-rearranged tumors, whereas pralsetinib has demonstrated promising results in an ongoing phase I clinical trial (NCT03037385) (39, 49). These data and our recent work on amivantamab, an EGFR-MET bispecific antibody for treatment of *EGFR* exon 20 insertions, underline feasibility of PDO-based preclinical studies (50).

This study had several limitations. It was a retrospective study based on extensive organoid biobanking and NGS. To expand clinical utility of organoids, future studies need to be

prospective and determine the time frame for organoids to be informative for clinical decision making. We also acknowledge that the predictive value of organoids needs to be validated in a large cohort.

In summary, we demonstrate that advanced lung adenocarcinoma organoids can recapitulate clinical responses to targeted therapies and facilitate development of novel therapeutic strategies. The clinical relevance of organoids will contribute to implementation of precision medicine.

References

1. Yang C-Y, Yang JC-H, Yang P-C. Precision management of advanced non–small cell lung cancer. *Annual review of medicine*. 2020;71:117-36.
2. National Comprehensive Cancer Network. Non-small cell lung cancer (version 8. 2020) [Available from: https://www.nccn.org/professionals/physician_gls/pdf/nscl.pdf.
3. Lim SM, Kim HR, Lee J-S, Lee KH, Lee Y-G, Min YJ, et al. Open-label, multicenter, phase II study of ceritinib in patients with non–small-cell lung cancer harboring ROS1 rearrangement. *Journal of Clinical Oncology*. 2017;35(23):2613-8.
4. Mok TS, Wu Y-L, Thongprasert S, Yang C-H, Chu D-T, Saijo N, et al. Gefitinib or carboplatin–paclitaxel in pulmonary adenocarcinoma. *New England Journal of Medicine*. 2009;361(10):947-57.
5. Planchard D, Besse B, Groen HJ, Souquet P-J, Quoix E, Baik CS, et al. Dabrafenib plus trametinib in patients with previously treated BRAFV600E-mutant metastatic non-small cell lung cancer: an open-label, multicentre phase 2 trial. *The Lancet Oncology*. 2016;17(7):984-93.
6. Galli G, Corrao G, Imbimbo M, Proto C, Signorelli D, Ganzinelli M, et al. Uncommon mutations in epidermal growth factor receptor and response to first and second generation tyrosine kinase inhibitors: a case series and literature review. *Lung Cancer*. 2018;115:135-42.
7. Kim S-Y, Lee JY, Kim DH, Joo H-S, Yun MR, Jung D, et al. Patient-derived cells to guide targeted therapy for advanced lung adenocarcinoma. *Scientific reports*. 2019;9(1):1-12.
8. Marchetti A, Felicioni L, Malatesta S, Grazia Sciarrotta M, Guetti L, Chella A, et al. Clinical features and outcome of patients with non-small-cell lung cancer harboring BRAF mutations. *J Clin Oncol*. 2011;29(26):3574-9.
9. Yao Z, Yaeger R, Rodrik-Outmezguine VS, Tao A, Torres NM, Chang MT, et al. Tumours with class 3 BRAF mutants are sensitive to the inhibition of activated RAS. *Nature*. 2017;548(7666):234-8.
10. Clevers H. Modeling development and disease with organoids. *Cell*. 2016;165(7):1586-97.
11. Crystal AS, Shaw AT, Sequist LV, Friboulet L, Niederst MJ, Lockerman EL, et al. Patient-derived models of acquired resistance can identify effective drug combinations for cancer. *Science*. 2014;346(6216):1480-6.
12. Siolas D, Hannon GJ. Patient-derived tumor xenografts: transforming clinical samples into mouse models. *Cancer research*. 2013;73(17):5315-9.
13. Dijkstra KK, Monkhorst K, Schipper LJ, Hartemink KJ, Smit EF, Kaing S, et al. Challenges in Establishing Pure Lung Cancer Organoids Limit Their Utility for Personalized Medicine. *Cell Rep*. 2020;31(5):107588.
14. Kim M, Mun H, Sung CO, Cho EJ, Jeon HJ, Chun SM, et al. Patient-derived lung cancer organoids as in vitro cancer models for therapeutic screening. *Nat Commun*. 2019;10(1):3991.
15. Sachs N, Papaspyropoulos A, Zomer-van Ommen DD, Heo I, Böttinger L, Klay D, et al. Long-term expanding human airway organoids for disease modeling. *The EMBO journal*. 2019;38(4):e100300.
16. Shi R, Radulovich N, Ng C, Liu N, Notsuda H, Cabanero M, et al. Organoid Cultures as Preclinical Models of Non-Small Cell Lung Cancer. *Clin Cancer Res*. 2020;26(5):1162-74.
17. Li H, Durbin R. Fast and accurate long-read alignment with Burrows–Wheeler transform. *Bioinformatics*. 2010;26(5):589-95.
18. Tso K-Y, Lee SD, Lo K-W, Yip KY. Are special read alignment strategies necessary and cost-effective when handling sequencing reads from patient-derived tumor xenografts? *BMC genomics*. 2014;15(1):1-11.

19. Ramos AH, Lichtenstein L, Gupta M, Lawrence MS, Pugh TJ, Saksena G, et al. Oncotator: cancer variant annotation tool. *Human mutation*. 2015;36(4):E2423-E9.
20. Talevich E, Shain AH, Botton T, Bastian BC. CNVkit: genome-wide copy number detection and visualization from targeted DNA sequencing. *PLoS computational biology*. 2016;12(4):e1004873.
21. Van Allen EM, Wagle N, Stojanov P, Perrin DL, Cibulskis K, Marlow S, et al. Whole-exome sequencing and clinical interpretation of formalin-fixed, paraffin-embedded tumor samples to guide precision cancer medicine. *Nature medicine*. 2014;20(6):682-8.
22. Roerink SF, Sasaki N, Lee-Six H, Young MD, Alexandrov LB, Behjati S, et al. Intra-tumour diversification in colorectal cancer at the single-cell level. *Nature*. 2018;556(7702):457-62.
23. Sharma SV, Lee DY, Li B, Quinlan MP, Takahashi F, Maheswaran S, et al. A chromatin-mediated reversible drug-tolerant state in cancer cell subpopulations. *Cell*. 2010;141(1):69-80.
24. Yun MR, Kim DH, Kim S-Y, Joo H-S, Lee YW, Choi HM, et al. Repotrectinib Exhibits Potent Antitumor Activity in Treatment-Naïve and Solvent-Front–Mutant ROS1-Rearranged Non–Small Cell Lung Cancer. *Clinical Cancer Research*. 2020;26(13):3287-95.
25. Leonetti A, Sharma S, Minari R, Perego P, Giovannetti E, Tiseo M. Resistance mechanisms to osimertinib in EGFR-mutated non-small cell lung cancer. *British journal of cancer*. 2019;121(9):725-37.
26. Walsh K, Wallace W, Butler R, Mackean M, Harrison D, Stirling D, et al. A cautionary lesson on the use of targeted methods for EGFR mutation analysis: a case report. *Journal of clinical pathology*. 2014;67(8):734-5.
27. Jänne PA, Yang JC-H, Kim D-W, Planchard D, Ohe Y, Ramalingam SS, et al. AZD9291 in EGFR inhibitor–resistant non–small-cell lung cancer. *New England Journal of Medicine*. 2015;372(18):1689-99.
28. Tiriac H, Belleau P, Engle DD, Plenker D, Deschenes A, Somerville TDD, et al. Organoid Profiling Identifies Common Responders to Chemotherapy in Pancreatic Cancer. *Cancer Discov*. 2018;8(9):1112-29.
29. Ooft SN, Weeber F, Dijkstra KK, McLean CM, Kaing S, van Werkhoven E, et al. Patient-derived organoids can predict response to chemotherapy in metastatic colorectal cancer patients. *Sci Transl Med*. 2019;11(513).
30. Fujita-Sato S, Galeas J, Truitt M, Pitt C, Urisman A, Bandyopadhyay S, et al. Enhanced MET translation and signaling sustains K-Ras–driven proliferation under anchorage-independent growth conditions. *Cancer research*. 2015;75(14):2851-62.
31. Breslin S, O'Driscoll L. The relevance of using 3D cell cultures, in addition to 2D monolayer cultures, when evaluating breast cancer drug sensitivity and resistance. *Oncotarget*. 2016;7(29):45745.
32. Pickl M, Ries C. Comparison of 3D and 2D tumor models reveals enhanced HER2 activation in 3D associated with an increased response to trastuzumab. *Oncogene*. 2009;28(3):461-8.
33. Moro L, Dolce L, Cabodi S, Bergatto E, Erba EB, Smeriglio M, et al. Integrin-induced epidermal growth factor (EGF) receptor activation requires c-Src and p130Cas and leads to phosphorylation of specific EGF receptor tyrosines. *Journal of Biological Chemistry*. 2002;277(11):9405-14.
34. Ochi N, Takigawa N, Harada D, Yasugi M, Ichihara E, Hotta K, et al. Src mediates ERK reactivation in gefitinib resistance in non-small cell lung cancer. *Experimental cell research*. 2014;322(1):168-77.
35. Song L, Morris M, Bagui T, Lee FY, Jove R, Haura EB. Dasatinib (BMS-354825) selectively induces apoptosis in lung cancer cells dependent on epidermal growth factor receptor signaling for survival. *Cancer research*. 2006;66(11):5542-8.

36. Uchibori K, Inase N, Araki M, Kamada M, Sato S, Okuno Y, et al. Brigatinib combined with anti-EGFR antibody overcomes osimertinib resistance in EGFR-mutated non-small-cell lung cancer. *Nature communications*. 2017;8(1):1-16.
37. Liang S-K, Ko J-C, Yang JC-H, Shih J-Y. Afatinib is effective in the treatment of lung adenocarcinoma with uncommon EGFR p. L747P and p. L747S mutations. *Lung Cancer*. 2019;133:103-9.
38. Robichaux JP, Elamin YY, Vijayan R, Nilsson MB, Hu L, He J, et al. Pan-cancer landscape and analysis of ERBB2 mutations identifies poziotinib as a clinically active inhibitor and enhancer of T-DM1 activity. *Cancer Cell*. 2019;36(4):444-57. e7.
39. Subbiah V, Gainor JF, Rahal R, Brubaker JD, Kim JL, Maynard M, et al. Precision targeted therapy with BLU-667 for RET-driven cancers. *Cancer discovery*. 2018;8(7):836-49.
40. Vlachogiannis G, Hedayat S, Vatsiou A, Jamin Y, Fernández-Mateos J, Khan K, et al. Patient-derived organoids model treatment response of metastatic gastrointestinal cancers. *Science*. 2018;359(6378):920-6.
41. Yao Y, Xu X, Yang L, Zhu J, Wan J, Shen L, et al. Patient-derived organoids predict chemoradiation responses of locally advanced rectal cancer. *Cell stem cell*. 2020;26(1):17-26. e6.
42. Fridman R, Benton G, Aranoutova I, Kleinman HK, Bonfil RD. Increased initiation and growth of tumor cell lines, cancer stem cells and biopsy material in mice using basement membrane matrix protein (Cultrex or Matrigel) co-injection. *nature protocols*. 2012;7(6):1138.
43. Zheng C, Sun Y-h, Ye X-l, Chen H-q, Ji H-b. Establishment and characterization of primary lung cancer cell lines from Chinese population. *Acta Pharmacologica Sinica*. 2011;32(3):385-92.
44. Ho C-C, Liao W-Y, Lin C-A, Shih J-Y, Yu C-J, Yang JC-H. Acquired BRAF V600E mutation as resistant mechanism after treatment with osimertinib. *Journal of Thoracic Oncology*. 2017;12(3):567-72.
45. Marconcini R, Galli L, Antonuzzo A, Bursi S, Roncella C, Fontanini G, et al. Metastatic BRAF K601E-mutated melanoma reaches complete response to MEK inhibitor trametinib administered for over 36 months. *Experimental hematology & oncology*. 2017;6(1):1-5.
46. Huang J, Wang Y, Zhai Y, Wang J. Non-small cell lung cancer harboring a rare EGFR L747P mutation showing intrinsic resistance to both gefitinib and osimertinib (AZD9291): A case report. *Thoracic cancer*. 2018;9(6):745-9.
47. Hyman DM, Piha-Paul SA, Won H, Rodon J, Saura C, Shapiro GI, et al. HER kinase inhibition in patients with HER2-and HER3-mutant cancers. *Nature*. 2018;554(7691):189-94.
48. Mazieres J, Peters S, Lepage B, Cortot AB, Barlesi F, Beau-Faller M, et al. Lung cancer that harbors an HER2 mutation: epidemiologic characteristics and therapeutic perspectives. *Journal of clinical oncology*. 2013;31(16):1997-2003.
49. Drilon A, Rekhtman N, Arcila M, Wang L, Ni A, Albano M, et al. Cabozantinib in patients with advanced RET-rearranged non-small-cell lung cancer: an open-label, single-centre, phase 2, single-arm trial. *The Lancet Oncology*. 2016;17(12):1653-60.
50. Yun J, Lee S-H, Kim S-Y, Jeong S-Y, Kim J-H, Pyo K-H, et al. Antitumor Activity of Amivantamab (JNJ-61186372), an EGFR–MET Bispecific Antibody, in Diverse Models of EGFR Exon 20 Insertion–Driven NSCLC. *Cancer discovery*. 2020;10(8):1194-209.

Acknowledgements

We thank the patients for their contributions to this study. Patient blood and FFPE samples were provided by the Biobank, Severance Hospital, Seoul, Korea. This work was supported by Interpark Bio Convergence Corp., Seoul, Korea and Science Research Program through the NRF funded by the Ministry of Science and ICT (2016R1A2B3016282). We also thank Dr. Koo (IMBA, Austria) for his advice on establishing organoids. The selection of clinically-relevant driver genes are in whole or part based upon data generated by the TCGA Research Network: https://www.cancer.gov/tcga.

Author contributions

Study design: SYK, HKK, BCC. Methodology: SYK, SMK, HKK. Acquisition of data: SYK, SMK, SmL, JYL, SJC, SDY, CGK, SRG, AYP, HKK, BCC. Interpretation of data: SYK, SMK, SmL, SJC, SDY, SGH, MRY, CGK, CwP, SML, SGH, HKK, BCC. Writing of the manuscript: SYK, SMK. Editing of the manuscript: HKK, BCC.

Figure legends

Figure 1. Establishment and characterization of patient-derived organoids from advanced lung adenocarcinoma. A) Representative H&E and IHC stained images of NSCLC organoids and their parental tumor tissues. The tumor organoids were positive for TTF-1, an adenocarcinoma marker, and negative for Calrectinin, a mesothelial cell marker. NSCLC organoids recapitulated morphological and histological features of original tumor tissues. H&E, brightfield, and IHC images are shown. Scale bar, 100 μm. B) Genomic landscape in 61 patient-derived organoids of advanced lung adenocarcinoma. Organoids were derived from TKI-naïve NSCLC, TKI-resistant NSCLC, NSCLC without driver oncogenes, and normal tissue. Clinically-relevant somatic alterations selected from the TARGET database are shown. Actionable targets and clinically-relevant driver genes based on the NCCN guideline (version 8.2020) and the lung adenocarcinoma TCGA database are indicated (left). Type of alteration is indicated by color codes. The percentage of organoids harboring the indicated alterations are shown (right). TTF-1, thyroid transcription factor 1; IHC, immunohistochemistry.

Figure 2. Advanced lung adenocarcinoma organoids can predict patient treatment responses to a TKI monotherapy. A) Swimmers' plot showing clinical annotations of 9 NSCLC patients who received subsequent TKI therapy after their tumor specimens were obtained to generate organoids. Each bar represents an individual patient. Subsequent TKI therapy each patient received is indicated on the right. B) Table summarizing correlations between clinical responses (PFS) in patients and *in vitro* responses (mean IC_{50} value from 3 independent experiments at 3 days) in matching PDOs. C) Bar graphs showing percentage change of cell viability in PDOs after exposure to each TKI at 100 nmol/L for 3 days. Bar colors represent each patient whose best response was stable disease (red) or partial response (blue) to the TKI. Data are presented as the mean ± SEM (n = 3). TKI, tyrosine kinase inhibitor; RECIST, response evaluation criteria in solid tumors; PFS, progression-free survival; PR, partial response; SD, stable disease; PDO, patient-derived organoids; IC_{50}, the half maximal concentration. See also Supplementary Table 2.

Figure 3. Drug sensitivity to gefitinib is associated with culture condition in YUO-004. A) Procedure for generating 2D PDOs. 3D PDOs were plated on collagen-coated plates and cultured in AO medium for more than a week up to 4 weeks. B) Comparison of IC_{50} values to the each TKI (top) between 3D and 2D PDOs (two-tailed Student *t*-test: n.s., not significant; **, $P<0.01$; ***, $P<0.005$). Red line denotes sensitive (IC_{50} value < 100 nmol/L) or resistant (IC_{50} value > 100 nmol/L) response to a drug. C) DNA chromatograms showing *EGFR* L747P mutation in 3D culture and 2D culture of YUO-050 and YUO-004. D) Scheme for model switching. 2D PDOs that were maintained as monolayer less than 4 weeks were

switched to 3D culture condition and cultured for up to 4 weeks. All models were maintained in AO medium. E) 3D, 2D, and 2D-3D cultures of YUO-050 and YUO-004 were treated with the indicated concentrations of gefitinib for 3 days. IC_{50} value of gefitinib is indicated for each culture condition (top). F) Representative immunoblots of indicated molecules in YUO-050 and YUO-004 at baseline. G) Representative immunoblots of indicated molecules in YUO-050 and YUO-004 at baseline. H) 3D YUO-050 and YUO-004 were treated with dasatinib alone, gefitinib alone, or gefitinib in combination with the indicated concentrations of dasatinib for 3 days. I) Representative immunoblots of indicated molecules in YUO-004 treated with the indicated concentration of gefitinib with or without dasatinib. In (B), (E) and (H), data are presented as the mean ± SEM (n = 3). AO, airway organoid medium.

Figure 4. Patient-derived organoids recapitulate a clinical response to dabrafenib/trametinib combination therapy against *EGFR* exon 19 deletion plus *BRAF* G464A mutation. A) Summary of next-generation sequencing analyses in liquid- and tissue biopsies and YUO-071. B) Computed tomography scans showing tumor (red arrows) at disease progression to osimertinib (left) and after dabrafenib plus trametinib combination therapy (right) in a patient from which YUO-071 was generated. C) YUO-071 was treated with the indicated concentrations of osimertinib (far left), cetuximab (left), brigatinib with or without cetuximab at the indicated concentrations (right), and dabrafenib alone, trametinib alone, or trametinib plus dabrafenib at the indicated concentrations (far right) for 5 days. D) YUO-071 was exposed to osimertinib, dabrafenib, trametinib, dabrafenib plus trametinib, cetuximab, brigatinib, cetuximab plus brigatinib at the indicated concentrations for 15 days (left). Relative cell viability of YUO-071 before (day 0) and after the long-term exposure (day 15) to dabrafenib plus trametinib is shown on the right panel. E) Representative immunofluorescence images of indicated molecules in YUO-071 treated with control or 100 nmol/L dabrafenib in combination with 100 nmol/L trametinib for 5 days. Scale bar, 100 μM. F) Bar graphs showing quantification of Ki-67-positive cells (left) and cleaved caspase 3-positive cells (right) in each group from (E). In (C), (D) and (F), data are presented as the mean ± SEM (n = 3) (two-tailed Student *t*-test). N/D, none detected.

Figure 5. Patient-derived organoids predict clinical activity of afatinib against *EGFR* L747P mutation. A) YUO-004 and YUO-050 were treated with the indicated concentrations of gefitinib, erlotinib, dacomitinib, afatinib, osimertinib, and lazertinib for 3 days. 1st generation EGFR-TKIs are colored in dark, 2nd generation EGFR-TKIs are in red, and 3rd generation EGFR-TKIs are in blue. Data are presented as the mean ± SEM (n = 3). B) Representative immunoblots of indicated molecules in YUO-004 and YUO-050 treated with the indicated concentrations of gefitinib, afatinib, and osimertinib for 6 hours. C) Tumor growth curve of YUO-004 xenografts treated with indicated drugs at 25 mg/kg once daily (n=6 per group)

(one-way ANOVA with Dunnett's post test: n.s., not significant; **, *P*<0.005 vs. vehicle; ##, *P*<0.01 vs. afatinib). D) Immunoblots of indicated molecules in tumor samples obtained from YUO-004 xenografts treated with vehicle, 25 mg/kg gefitinib, afatinib, and osimertinib for 30 days. TGI, tumor growth inhibition.

Figure 6. Patient-derived organoids can identify effective therapies for advanced lung adenocarcinoma harboring *ERBB2* exon 20 insertions or *RET* rearrangements. A) YUO-046 and YUO-058 harboring *ERBB2* exon 20 insertions were treated with the indicated concentrations of gefitinib, lapatinib, neratinib, afatinib, and poziotinib for 5 days. B) Representative immunoblots of indicated molecules in YUO-046 and YUO-058 treated with the indicated concentrations of gefitinib, lapatinib, neratinib, afatinib, and poziotinib for 6 hours. C) IC_{50} values of gefitinib, lapatinib, neratinib, afatinib, and poziotinib in YUO-053, a normal-like organoid, and tumor organoids harboring *ERBB2* exon 20 insertions. D) Bar graphs showing mean relative IC_{50} values of the ERBB2 inhibitors in *ERBB2*-mutant organoids to the normal organoid. E) YUO-017 and YUO-049 harboring *RET* fusions were treated with the indicated concentrations of vandetanib, lenvatinib, cabozantinib, and pralsetinib for 5 days. F) Representative immunoblots of indicated molecules in YUO-017 and YUO-049 treated with the indicated concentrations of cabozantinib, pralsetinib, vandetanib, and lenvatinib for 2 hours. G) IC_{50} values of vandetanib, lenvatinib, cabozantinib, and pralsetinib in a normal-like organoid and tumor organoids harboring *RET*-arrangements. H) Bar graphs showing mean relative IC_{50} values of the RET inhibitors in *RET* fusion positive organoids to the normal organoid. In (A) and (E), data are presented as the mean ± SEM (n = 3). In (C) and (G), mean IC_{50} values were calculated from 3 biological replicates (3 technical replicates per independent experiment) using GraphPad Prism. In (D) and (H), data are presented as the mean ± SD (n = 2).

Figure 1.

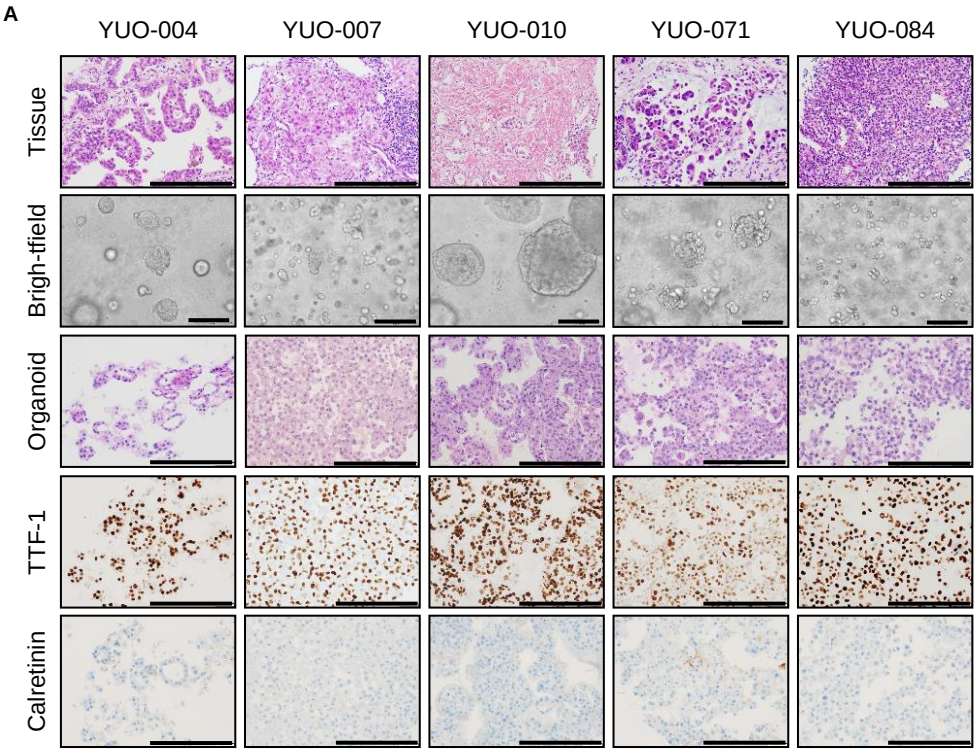

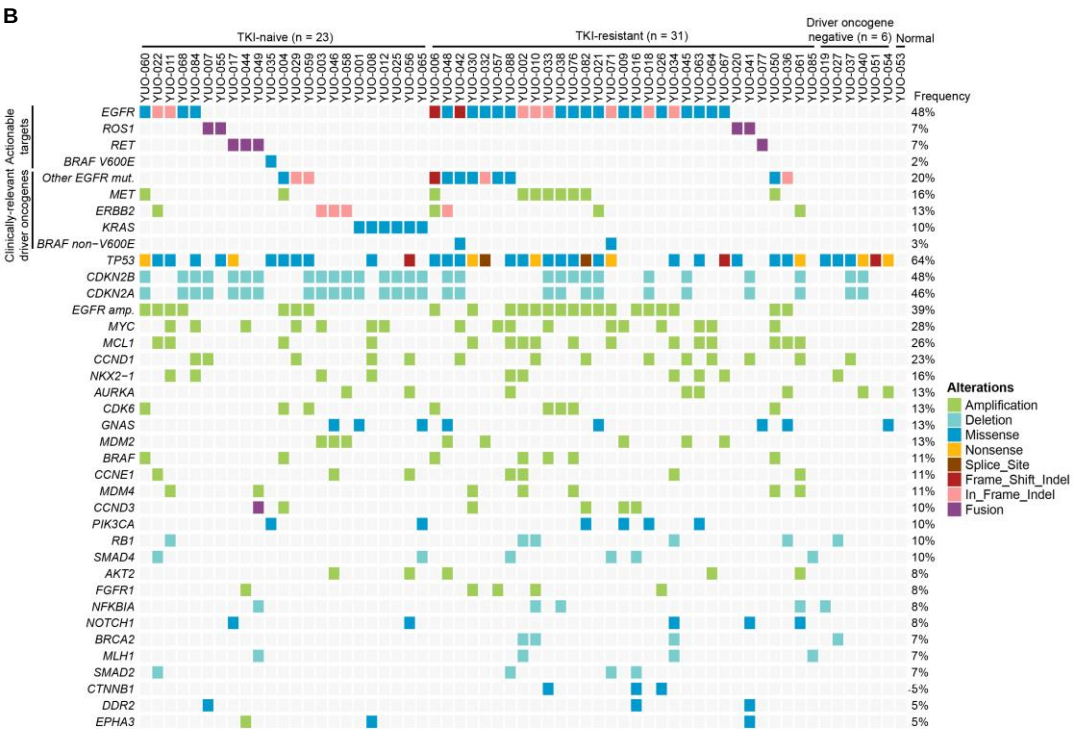

Figure 2.

A

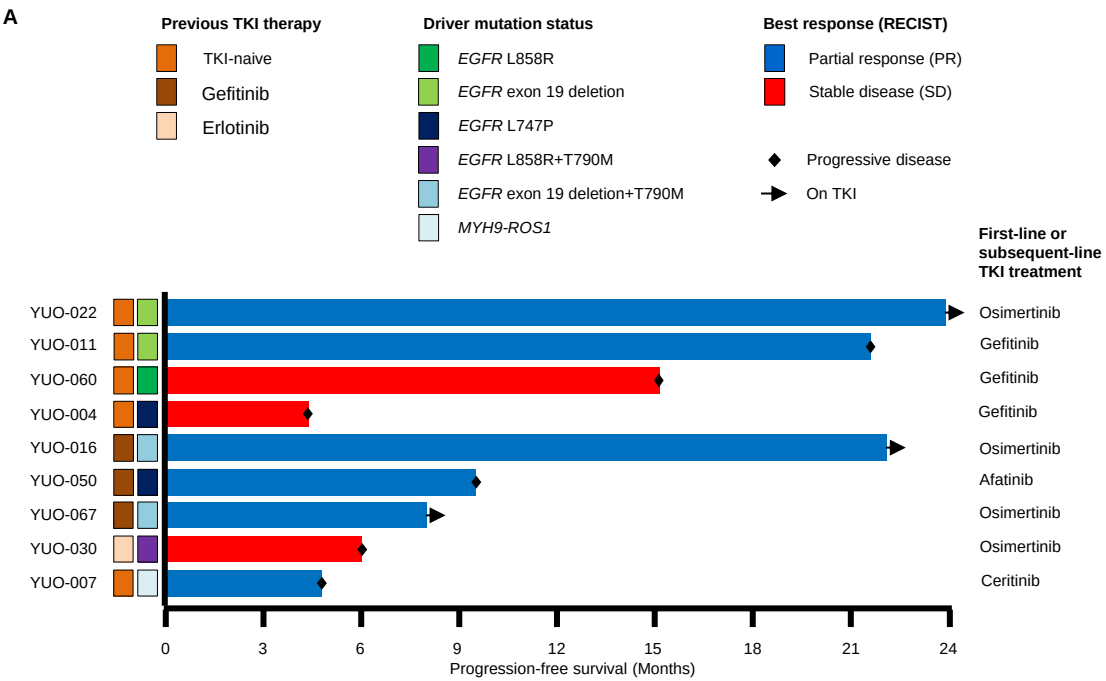

B

Overall		Patient (PFS)		
		< 9 months	> 9 months	Total
PDO (IC_{50})	Resistant	2	1	3
	Sensitive	1	4	5
	Total	3	5	8

C

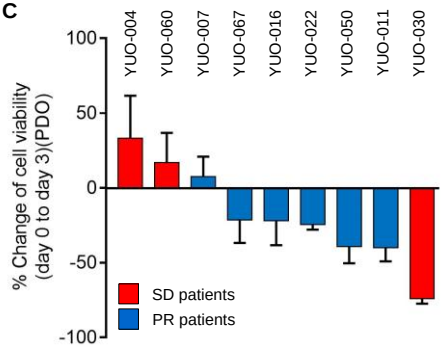

Figure 3.

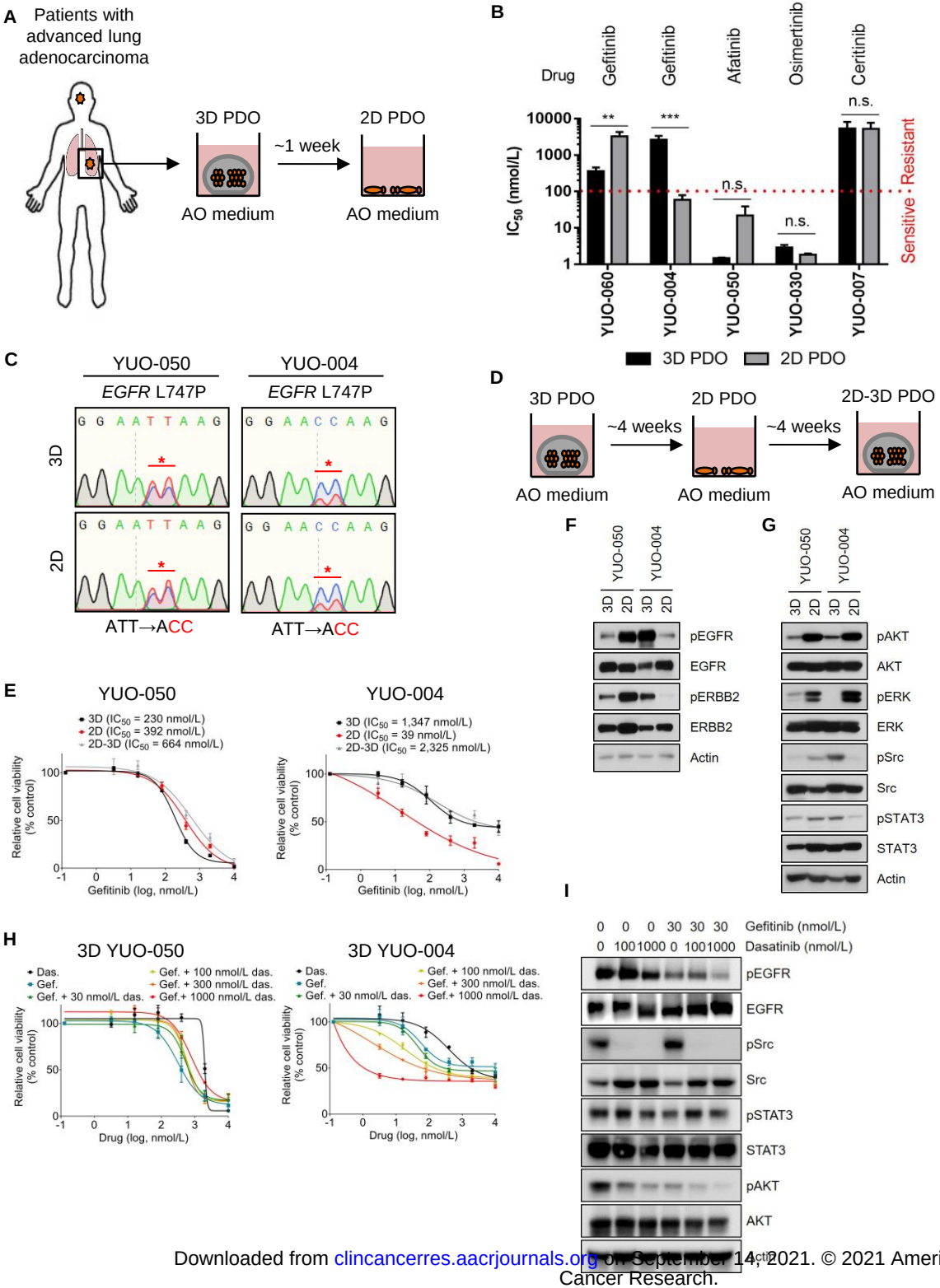

Figure 4.

A

Mutation	Plasma NGS	Tissue NGS	PDO NGS
EGFR ex 19 del	19.00%	21.85%	58.70%
EGFR T790M	0.10%	N/D	N/D
EGFR C797S	0.10%	N/D	N/D
TP53 R342*	5.80%	10.08%	56.60%
TP53 E56fs	6.00%	8.58%	50.80%
BRAF G464A	3.30%	5.37%	42.90%
BRAF V600E	0.30%	N/D	N/D

B

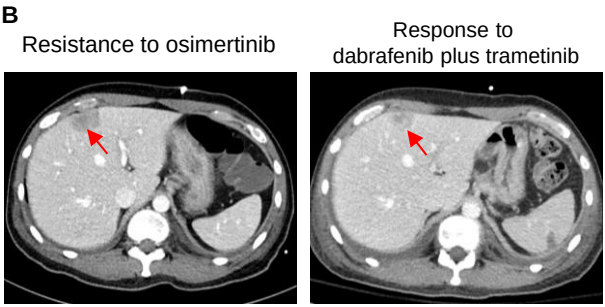

C

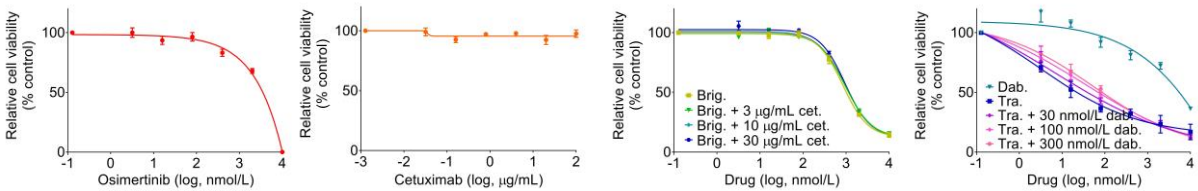

D

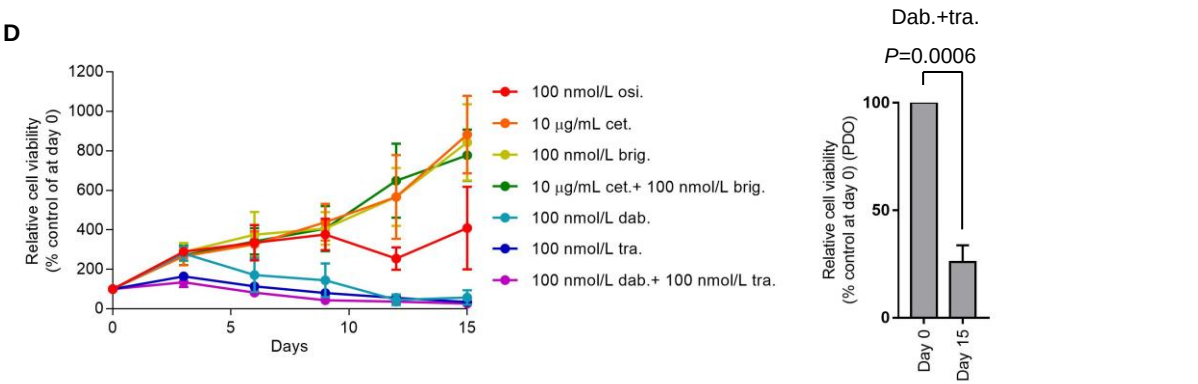

E

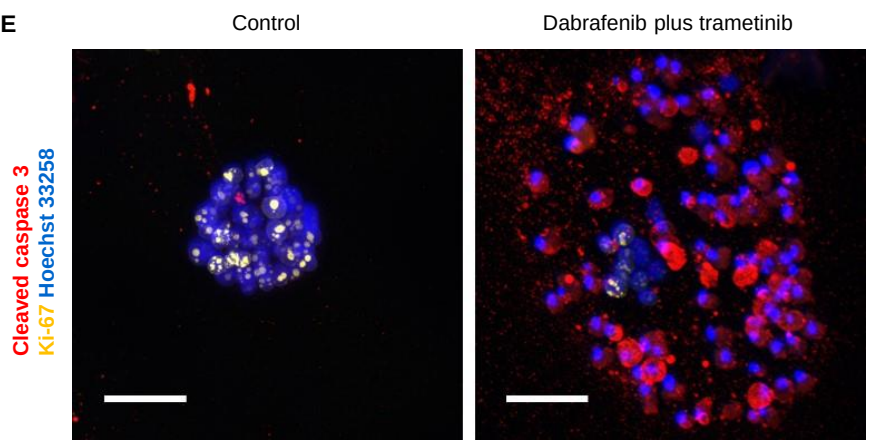

F

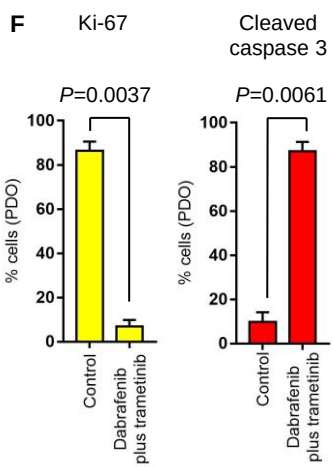

Figure 5.

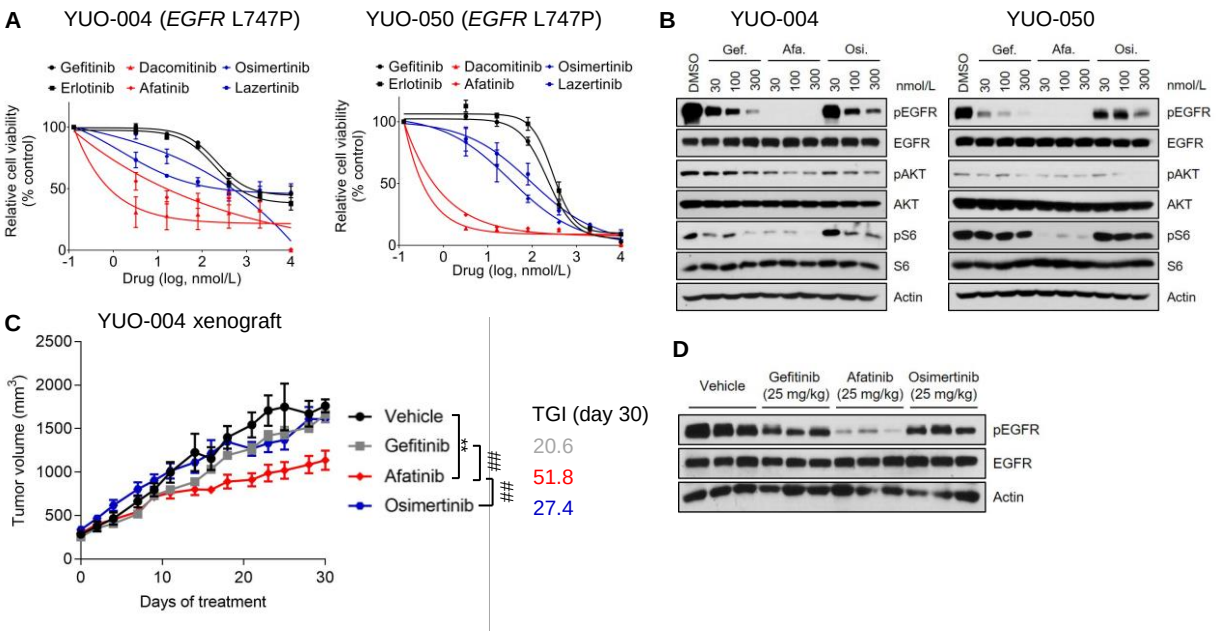

Figure 6.

A YUO-046 (*ERBB2* G778_779insCPG) YUO-058 (*ERBB2* A775_G779insYVMA)

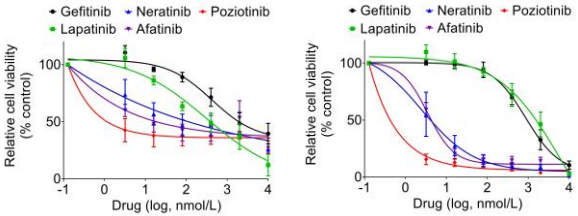

B YUO-046 YUO-058

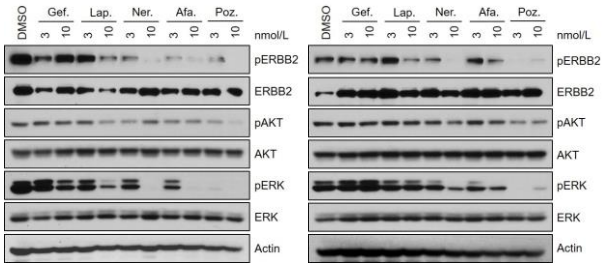

C

PDO ID	Type	Drug, mean IC_{50} (nmol/L)				
		Gefitinib	Lapatinib	Neratinib	Afatinib	Poziotinib
YUO-053	Normal	1026.0	596.3	363.3	46.6	14.2
YUO-046	Tumor	2275.0	388.5	109.2	27.7	5.6
YUO-058	Tumor	974.7	1289.0	5.0	4.8	1.0

D

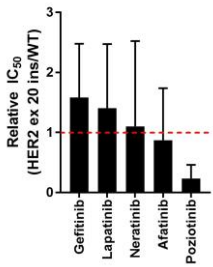

E YUO-017 (*CCDC6-RET*) YUO-049 (*KIF5B-RET*)

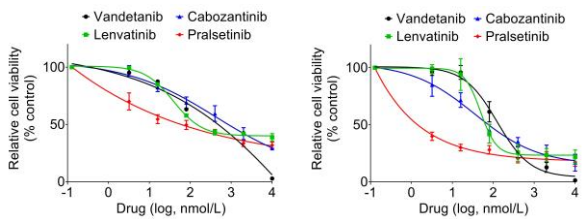

F YUO-017 YUO-049

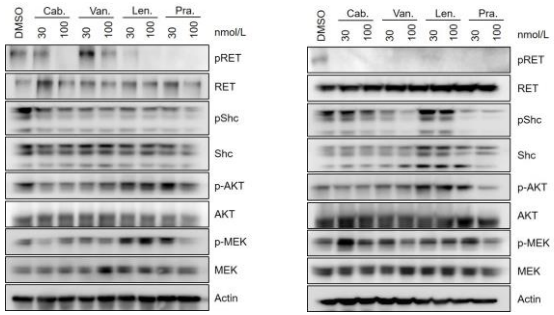

G

PDO ID	Type	Drug, mean IC_{50} (nmol/L)			
		Vandetanib	Lenvantinib	Cabozantinib	Pralsetinib
YUO-053	Normal	1069.9	7968.7	8287.7	8131
YUO-017	Tumor	314.1	323.2	880.4	79.8
YUO-049	Tumor	145.4	97	84.2	3.5

H

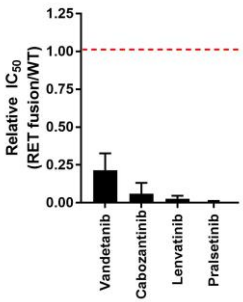

AACR American Association for Cancer Research

Clinical Cancer Research

Modeling clinical responses to targeted therapies by patient-derived organoids of advanced lung adenocarcinoma

Seok-Young Kim, Sang-Min Kim, Sumin Lim, et al.

Clin Cancer Res Published OnlineFirst June 3, 2021.